THE RESPONSE OF THE GENERAL CIRCULATION TO DEFORESTATION IN THE TROPICS

P.A. Dirmeyer and J. Shukla

1994

American Meteorology Society

Proc. 5th Symposium on Global Change

Pages 131-134

THE RESPONSE OF THE GENERAL CIRCULATION TO DEFORESTATION IN THE TROPICS

Paul A. Dirmeyer and J. Shukla

Center for Ocean-Land-Atmosphere Studies
Calverton, Maryland

1. INTRODUCTION

Much has been written about the potential effects of tropical deforestation on the surface energy balance and hydrological cycle (e.g., Henderson-Sellers and Gorintz, 1984; Dickinson and Henderson-Sellers, 1988; Lean and Warrilow, 1989; Nobre et al., 1991; Henderson-Sellers et al., 1993). However, little attention has been given to the effects of deforestation on the general circulation. In particular, it is of interest to determine what general changes in circulation are common to a number of experiments and scenarios. Spurious or case-dependent anomalies should be de-emphasized, and the genuine anomalies should be accentuated. Knowledge of systematic responses could help in pinpointing the mechanisms involved, and serve as a basis for prediction of regional as well as local climate changes induced by deforestation.

The results of four different sets of experiments are used in determining the general response of the general circulation to deforestation in the tropics. The one-year integrations of Shukla et al. (1990) and Nobre et al. (1991) (hereafter referred to as NSS) comprise one set. The other sets are one follow-up experiment with improved representation of SSTs and cloudiness, and two sets of four-year integrations with a lower horizontal resolution (Dirmeyer, 1992; Dirmeyer and Shukla, 1994). One of these sets has idealized topography.

2. DESCRIPTION OF EXPERIMENTS

In all experiments, an atmospheric general circulation model is used with specified lower boundary conditions over ocean and a biosphere model over land. The atmospheric general circulation model (GCM) used is a research version of the National Meteorological Center (NMC) global spectral model described by Sela (1980) with modifications and boundary [illegible] by Kanamitsu [illegible] NSS. The model is discretized into 18 vertical layers with resolution concentrated near the lower boundary. The complete physics package is used, including diurnally varying radiation. A Gaussian grid is used by the model for all physics calculations.

Table 1 shows the basic differences among the four sets of experiments. The lower boundary conditions for the GCM are supplied as follows. NSS used the Simple Biosphere (SiB) model of Sellers et al. (1986). The other experiments use a simplified version of SiB that is described by Xue et al. (1991), referred to hereafter as SSiB. The newer integrations have seasonally varying climatological sea surface temperatures. This is in contrast to NSS, where SSTs were held at December values throughout the integration.

There are other differences between these experiments and NSS. The current version of the GCM has interactive model-generated cloud

Table 1 Characteristics of the sets of experiments. See text for details.

	NSS	R40	R15	Ideal.
Resol.	R40	R40	R15	R15
Length	≈1y	14m	4y	4y
SST	fixed	clim.	clim.	clim.
Cloud	zon. avg.	Hou / zon. avg.	Hou	Hou
Orog.	earth	earth	earth	ideal.
Veg.	SiB	SSiB	SSiB	SSiB
Defor. $\Delta\alpha$	+.10	+.10 +.03	+.11 -.03	+.09 +.06 +.00

Corresponding author address: Paul A. Dirmeyer, Center for Ocean-Land-Atmosphere Studies, 4041 Powder Mill Road, Suite 302, Calverton, MD 20705

scheme of Hou (1990), whereas in NSS clouds were specified as a function of latitude and time of year. In addition, the specification of the "degraded grassland" vegetation in the deforested region is slightly different from that of NSS, because of a change from SiB to SSiB. In particular, several different albedos are used in the various deforestation integrations.

NSS and its follow-up integration are at R-40 resolution for one model year; the other two experiments are R-15 and four years duration. In three of the experiments, earth topography and vegetation are used, and tropical deforestation is specified to occur over the entire rainforest area of the Amazon basin. The lower boundary of one R-15 experiment is ocean covered except for a single, flat, rectangular continent centered on the equator. The continent spans 60° longitude by about 27° latitude, and is covered by a single vegetation type; rainforest in the control case, and degraded grass in the deforested cases. Figure 1 shows the geometry and areas of deforestation for each configuration.

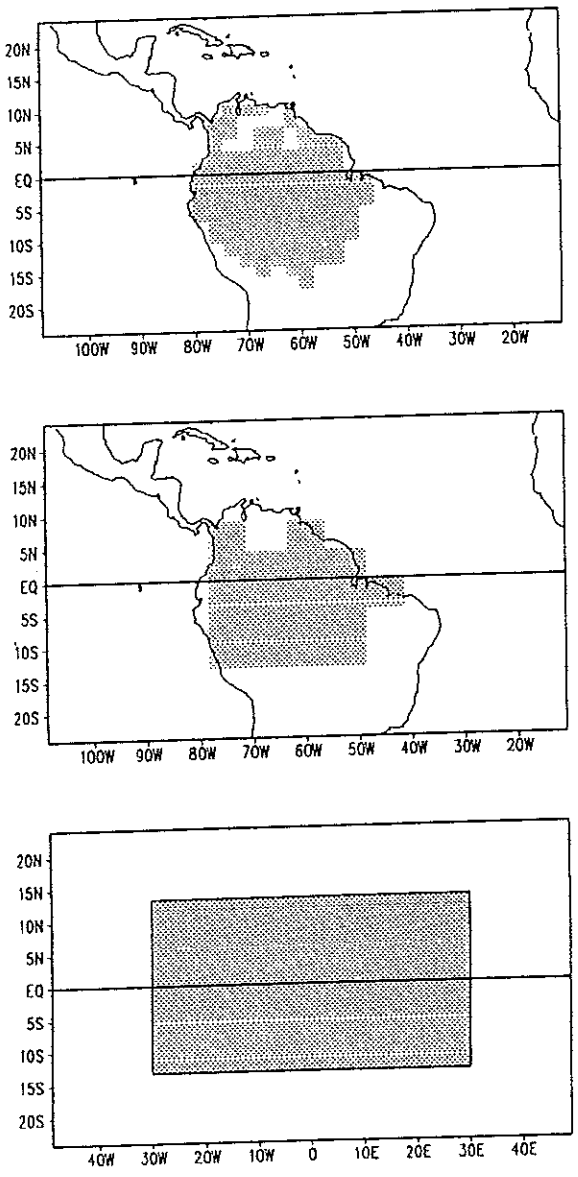

Figure 1 Orographic height (m) and areas of rainforest/deforestation for (a) R-40 cases and (b) R-15 cases with realistic topography; (c) R-15 with idealized topography.

3. RESULTS

Results for the Amazon deforestation experiments and the experiment with idealized topography will be presented separately. A synthesis of the changes in circulation will be presented at the end of the section.

3.1 *Amazon Deforestation*

Some features of the anomalous flow caused by deforestation are consistent among all experiments. Figure 2 is a schematic showing these features. Shaded arrows and letters represent the lower troposphere; unshaded features upper troposphere; A anticyclone; C cyclone. The most robust feature is a tendency for increased low-level flow westward from the tropical Atlantic over the Amazon basin. This feature is evident in the annual and seasonal averages of every experiment. This inflow region is straddled by a pair of ridges to the north and south.

The flow anomalies in the upper troposphere vary considerably between cases. At 300 mb, anticyclone pairs occur when net surface albedo changes little from forest values. Cyclone couplets tend to appear when surface albedo increases are great. One consistent feature is a tendency for westerly anomalies over the basin, particularly south of the Equator.

The relative dominance of lifting and sinking motion over the region of deforestation is also proportional to the change in albedo. Subsidence anomalies dominate the Amazon region when albedo is increased. Lifting is enhanced when grassland albedo is near that of rainforest. There is a fair amount of variability in the pattern of the anomalies between cases, and between years in the multi-year integrations. Nonetheless, there is a tendency in all cases with predicted clouds for lifting anomalies to occur over the eastern half of the basin, and sinking anomalies to occur in the west. Likewise, posi-

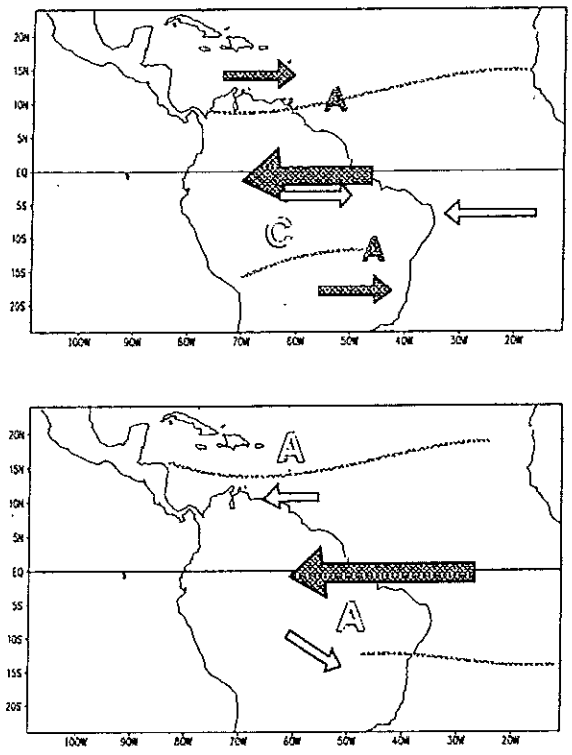

Figure 2 Schematic of flow anomalies caused by Amazon deforestation with large albedo increase (top) and no albedo increase (bottom). See text for details.

tive precipitation anomalies tend to occur near the Atlantic coast, and negative anomalies are more prevalent inland. This dipole is most obvious in the lower resolution case, although the pattern is apparent in the R-40 case after small-scale features are filtered out.

3.2 *Idealized Orography*

The annual mean anomaly patterns for the idealized topography case lack hemispheric asymmetry. Figure 3 shows the annual mean flow anomalies at 950 mb for high-albedo and low-albedo deforestation. There is still a strong tendency for easterly anomalies over the continent at low levels. Only in the low-albedo case is there any evidence of inflow from the west. Again, anomalous ridges flank the easterly anomaly in both cases, but the low-albedo flow strongly tends toward low-level convergence, while high-albedo deforestation promotes divergence near the surface.

The response in the upper troposphere (not shown) compliments the low-level flow. The high-albedo case is dominated by upper-level convergence between a pair of cyclones situated over the north and south coasts. An anticyclone couplet anomaly dominates the low-albedo case, with strong anomalous divergence aloft. In each case, most of the magnitude of the anomalies occurs in the zonal wind, implying a change in the climatological "Walker" circulation. Anomalies in vertical motion maxima and minima along the equator exceed 20% of the climatological values. There is also a substantial change in the zonally averaged meridional circulation, exceeding 10% at the climatological extrema.

In the low-albedo deforestation case, strong lifting anomalies are centered over the continent, with weak subsidence over the eastern coast. In the case of high-albedo deforestation, the subsidence over the eastern part of the continent dominates, and is joined by a second region over the western half. There is a lifting anomaly over the west coast.

3.3 *Synthesis of Responses*

There is a clear tendency for tropical deforestation to cause an increase in the strength of equatorial easterly flow onshore in the lower troposphere. This increases the advection of moisture over the continent. However, where that moisture is precipitated depends on the distribution of vertical motion anomalies, and thus low-level convergence and divergence. That seems to be very dependent on the geometry of the continent. As a result, the flow anomalies in the upper troposphere are also highly variable. In the experiments with a flat rectangular continent, lifting anomalies occur over the center of the land mass at the center of anomalous surface heating. There is no mechanism for orographic lifting, and roughness is small. Sinking anomalies occur near the east and west coasts, where zonal contrasts between land and sea are strong. In the low-albedo case, lifting dominates as heating and low-level convergence are strong. In the high-albedo case, the surface energy deficit encourages lifting to occur offshore, and subsidence is forced just inland from the coasts. In the Amazon experiments, anomalous heating is centered in the western half of the basin. The anomalous inflow is forced upward by orography near the coast, increasing rainfall there. The air which reaches the western Amazon has less moist static energy, and lifting is suppressed there. The presence of the Andes, and the hemispheric asymmetry of the heating encourages the flow to curl into the Southern Hemisphere

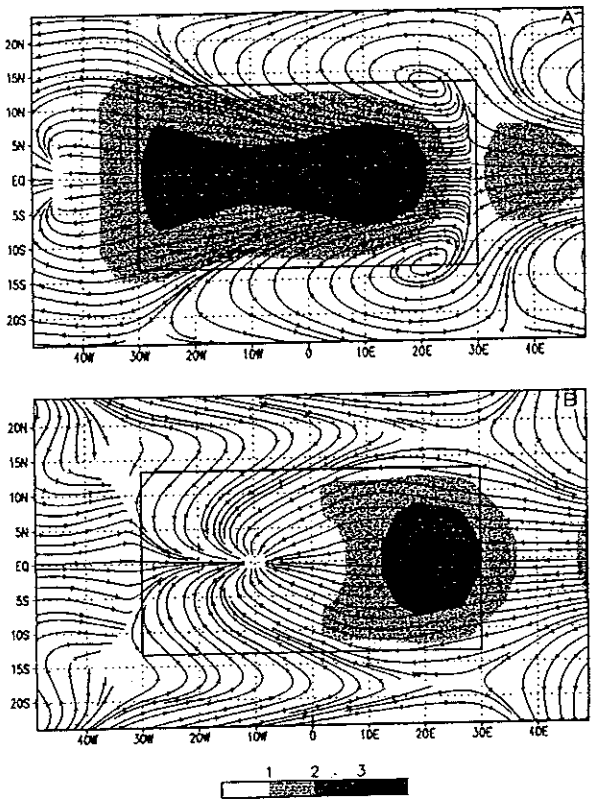

Figure 3 Annual mean flow anomalies at 950 mb in m s^{-1}; a) large albedo increase; b) slight albedo decrease.

around the South Atlantic subtropical ridge. These features are dictated by the geometry. Their relative strengths vary depending on the surface albedo and its effects on the energy balance. Again, low albedos bolster the lifting anomalies, while high albedos encourage sinking.

4. DISCUSSION

Many features of the horizontal flow are similar between experiments despite differences in resolution and geometry. The net effect on vertical motion due to variations in the surface albedo is also robust across experiments. However, the exact positions of vertical motion anomalies seems to between cases. For example, the tendency for sinking in the east and lifting to the west in the case with idealized orography is opposite that found for Amazon deforestation, suggesting that the exact position of anomalies in the divergence field are strongly governed by the geometry of the region. This presents problems in making universal statements about changes in rainfall, as precipitation anomalies correlate strongly with anomalies in vertical motion. High-albedo deforestation appears to decrease net rainfall, and deforestation with little or no albedo change may not reduce net rainfall at all. However, localities may see large anomalies of either sign. It cannot be determined from other published studies whether these features are common to all deforestation simulations.

References

Dickinson, R. E., and A. Henderson-Sellers, 1988: Modeling tropical deforestation: A study of land-surface parameterizations. *Quart. J. Roy. Meteor. Soc.*, 114, 439-462.

Dirmeyer, P. A., 1992: GCM studies of the influence of vegetation on the general circulation. PhD Dissertation, [Available from University of Maryland, College Park, MD 20742], 227pp.

Dirmeyer, P. A., and J. Shukla, 1994: Albedo as a modulator of climate response to tropical deforestation. *J. Climate* (submitted).

Henderson-Sellers, A., and V. Gornitz, 1984: Possible climatic impacts of land cover transformations, with particular emphasis on tropical deforestation. *Clim. Change*, 6, 231-258.

Henderson-Sellers, A., R. E. Dickinson, T. B. Durbidge, P. J. Kennedy, K. McGuffie, and A. J. Pitman, 1993: Tropical deforestation: Modeling local to regional scale climate change. *J. Geophys. Res.*, 98, 7289-7316.

Hou, Y.-T., 1990: Cloud-radiation-dynamics interaction. PhD Dissertation, [Available from University of Maryland, College Park, MD 20742], 209pp.

Kinter, J. L., J. Shukla, L. Marx and E. K. Schneider, 1988: A simulation of the winter and summer circulations with the NMC global circulation model. *J. Atmos. Sci.*, 45, 2486-2522.

Lean, J., and D. A. Warrilow, 1989: Simulation of the regional climatic impact of Amazon deforestation. *Nature*, 342, 411-413.

Nobre, C. A., P. J. Sellers, and J. Shukla, 1991: Amazonian deforestation and regional climate change. *J. Climate*, 4, 957-988.

Sela, J. G., 1980: Spectral modeling at the National Meteorological Center. *Mon. Wea. Rev.*, 108, 1279-1292.

Sellers, P. J., Y. Mintz, Y. C. Sud, and A. Dalcher, 1986: A simple biosphere model (SiB) for use within general circulation models. *J. Atmos. Sci.*, 43, 505-531.

Shukla, J., C. Nobre, and P. J. Sellers, 1990: Amazon deforestation and climate change. *Science*, 247, 1322-1325.

Xue, Y., P. J. Sellers, J. L. Kinter and J. Shukla, 1991, A simplified biosphere model for global climate studies: ,*J. Climate*, 4. 345-364.